JACS
JOURNAL OF THE AMERICAN CHEMICAL SOCIETY

Article

pubs.acs.org/JACS

Electronic and Spectroscopic Properties of Avobenzone Derivatives Attached to Mo_2 Quadruple Bonds: Suppression of the Photochemical Enol-to-Keto Transformation

Malcolm H. Chisholm,* Christopher B. Durr, Terry L. Gustafson,* William T. Kender, Thomas F. Spilker, and Philip J. Young

Department of Chemistry and Biochemistry, The Ohio State University, 100 West 18th Avenue, Columbus, Ohio 43210, United States

Supporting Information

ABSTRACT: From the reactions between $Mo_2(T^iPB)_4$, where T^iPB is 2,4,6-triisopropylbenzoate, and 2 equiv of the acids 4-formylbenzoic acid, HBzald; 4-(3-oxo-3-phenylpropanoyl)benzoic acid, HAvo; and 4-(2,2-difluoro-6-phenyl-2*H*-1λ^3,3,2λ^4-dioxaborinin-4-yl)benzoic acid, $HAvoBF_2$, the compounds $Mo_2(T^iPB)_2(Bzald)_2$, **I**; $Mo_2(T^iPB)_2(Avo)_2$, **II**; and $Mo_2(T^iPB)_2(AvoBF_2)_2$, **III**, have been isolated. Compounds **I** and **II** are red, and compound **III** is blue. The new compounds have been characterized by ^1H NMR, MALDI-TOF MS, steady-state absorption and emission spectroscopies, and femtosecond and nanosecond time-resolved transient absorption and infrared spectroscopies. Electronic structure calculations employing density functional theory and time-dependent density functional theory have been carried out to aid in the interpretation of these data. These compounds have strong metal-to-ligand charge transfer, MLCT, and transitions in the visible region of their spectra, and these comprise the S_1 states having lifetimes ~5−15 ps. The triplet states are $Mo_2\delta\delta^*$ with lifetimes in the microseconds. The spectroscopic properties of **I** and **II** are similar, whereas the planarity of the ligand in **III** greatly lowers the energy of the MLCT and enhances the intensity of the time-resolved spectra. The Mo_2 unit shifts the ground state equilibrium entirely to the enol form and quenches the degradation pathways of the avobenzone moiety.

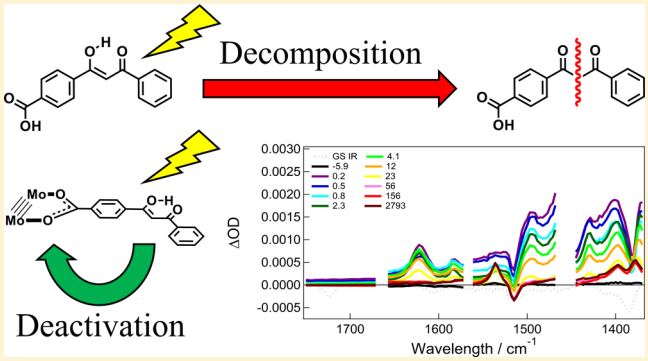

INTRODUCTION

Avobenzone, a UVA filter commonly employed in sunscreens, has been extensively studied because of its unique ground state enol−keto tautomerization in solution.[1,2] The enol predominates in this equilibrium, but it can be shifted in favor of the keto by exciting the molecule with UV light.[3−7] This photoinduced conformation change is of interest because of its potential as a photoswitch as well as the effect it has on the excited state dynamics. In addition, this tautomerization is relevant to the use of avobenzone in sunscreen. Avobenzone has been shown to decompose into potentially toxic byproducts via a complicated light-activated process.[8] Complete understanding of this process is essential for incorporating the conformation change with transition metals as well as for preventing decomposition of avobenzone. With the inclusion of a carboxylic acid moiety, avobenzone derivatives can be attached to transition metal complexes without changing the molecular structure. This allows for the study of avobenzone analogues in new electronic environments. It is of interest to note that photoisomerization of organic molecules and changes in the excited state dynamics upon coordination to metal carbonyl complexes have been investigated using ultrafast time-resolved infrared (TRIR).[9] These studies have focused primarily on the sensitization of isomerization by means of the metal complexes, whereas the current study introduces an avenue to deactivation.

Carboxylate ligands attached to Mo_2 quadruply bonded centers have been previously studied.[10] Compounds of the general formula *trans*-$Mo_2L_2L'_2$, where L′ is 2,4,6-triisopropylbenzoate (T^iPB) and L is a π-acceptor, such as cyanobenzoate[11] or cyanoacrylate,[12] have been shown to exhibit strong, fully allowed $Mo_2\delta$ to ligand π^* (MLCT) transitions in the visible and into the near-infrared region of the electromagnetic spectrum. By using tungsten as the metal center, the band can be extended as far as 1200 nm. The trans disposition gives rise to extended Lπ-$Mo_2\delta$-Lπ conjugation, making it the thermodynamically favored configuration. These complexes typically have relatively long S_1 state lifetimes in the range of 1−15 ps and T_1 states (most frequently $^3Mo_2\delta\delta^*$) with lifetimes on the microsecond time scale. Their excited state dynamics can be probed using nanosecond (ns) and

Received: February 10, 2015
Published: April 9, 2015

DOI: 10.1021/jacs.5b01495
J. Am. Chem. Soc. 2015, 137, 5155−5162

femtosecond (fs) transient absorption and time-resolved infrared spectroscopies.

The Mo_2 centers are an ideal scaffold to investigate a number of different ligands because of facile attachment of new ligands through a CO_2 functional group. Recently, the photophysical properties of arylboron compounds have been an area of focused research. The influence on the electronic structure of a diarylboron moiety attached to a benzoate ligand was previously investigated for these Mo_2 systems.[13] Another arylboron molecule is the BODIPY fluorophore (Scheme 1)

Scheme 1. Structures of BODIPY (left) and Avobenzone (right)

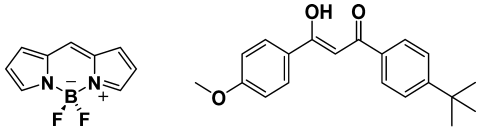

BODIPY Avobenzone

which exhibits sharp and intense spectral features due to its rigid structure.[14] The diketone functionality of avobenzone derivatives makes them suitable for coordination of a BF_2 unit, giving rise to a structure similar to BODIPY.[15]

RESULTS AND DISCUSSION

We were interested in investigating the effect of both the enol−keto tautomerization and incorporation of a BF_2 unit into a Mo_2 paddlewheel system and herein report on studies that were prompted by these considerations.

Syntheses. *Ligands.* The carboxylic acids employed in the synthesis of the new molybdenum compounds are shown in Chart 1, along with their formal names and the abbreviations used in this paper.

Of the carboxylic acids, only HBzald is commercially available, and the syntheses of the other two are shown in Scheme 2.[16]

The molybdenum compounds were made from the reactions between $Mo_2(T^iPB)_4$, where T^iPB = 2,4,6-triisopropylbenzoate, and 2 equiv of the appropriate carboxylic acid, as shown in eq 1.

$$Mo_2(T^iPB)_4 + 2LH \xrightarrow[RT,3days]{\text{tolune}} \textit{trans}\text{-}Mo_2(T^iPB)_2L_2 + 2T^iPBH \quad (1)$$

The new compounds gave molecular ions by MALDI-TOF mass spectrometry (Supporting Information Figures S1−S3), and their ^1H NMR data conformed to expectations as members of a now extensive series of compounds of the form *trans*-$Mo_2(T^iPB)_2L_2$, where L = a conjugated carboxylate. Details pertaining to the synthesis and characterization data are given in the Experimental part of the Supporting Information.

Single Crystal X-ray Structure of I. An ORTEP drawing of the molecular structure of **I** can be seen in Figure 1, and a table of selected crystallographic data can be seen in Supporting Information Table S1. The phenyl ring associated with the T^iPB moiety is twisted out of conjugation with the $-CO_2$ unit, with a torsion angle of 81.4°. The benzaldehyde ligand, however, is coplanar with the attendant $-CO_2$ unit with a torsion angle of 5.5°. A full description of the structural solution and refinement of **I** can be found in the Supporting Information. Although no molecular structure determination was carried out for compounds **II** or **III** in this work, previous studies have shown that T^iPB ligands enforce the trans geometry of the type *trans*-$Mo_2(T^iPB)_2L_2$. In each of these, the aryl planes of the T^iPB ligands are twisted close to 90° from the plane of their respective carboxylate units, whereas the *trans*-L ligands lie in a plane facilitating $L\pi$-$Mo_2\delta$-$L\pi$ conjugation.

Electronic Structural Calculations. To aid in the interpretation of the spectral data, electronic structural calculations employing density functional theory were carried out on model compounds in which formate was substituted for the bulky $T^{iP}B$ ligands. This was done to reduce computing time and has been shown in previous works to result in minimal difference for the calculation results because the T^iPB ligands are twisted 90° out of conjugation.[17] The model compounds bearing the Bzald, Avo, and $AvoBF_2$ ligands are denoted **I′**, **II′**, and **III′** respectively; however, the Avo ligand can exist in either the enol or keto form, and consequently, calculations were carried out for both. As we shall show from experimental evidence, the predominant form present in solution is the enol form. This is present in >97%, based on ^1H NMR data.

It is instructive to compare the calculated frontier molecular orbitals of **I′** and the keto form of **II′**; these are shown in

Chart 1. Structure, Formal Name, and Abbreviations of the Three Ligands Used in This Paper

Structure	Abbreviation	Formal Name
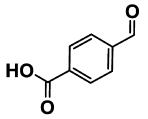	HBzald	4-formylbenzoic acid
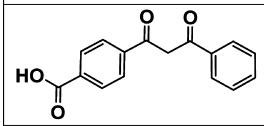	HAvo	4-(3-oxo-3-phenylpropanoyl)benzoic acid
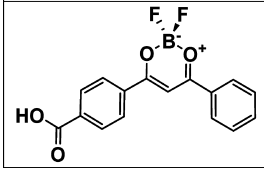	$HAvoBF_2$	4-(2,2-difluoro-6-phenyl-2*H*-1λ³,3,2λ⁴-dioxaborinin-4-yl)benzoic acid

DOI: 10.1021/jacs.5b01495
J. Am. Chem. Soc. 2015, 137, 5155−5162

Scheme 2. Syntheses of Ligands HAvo and $HAvoBF_2$

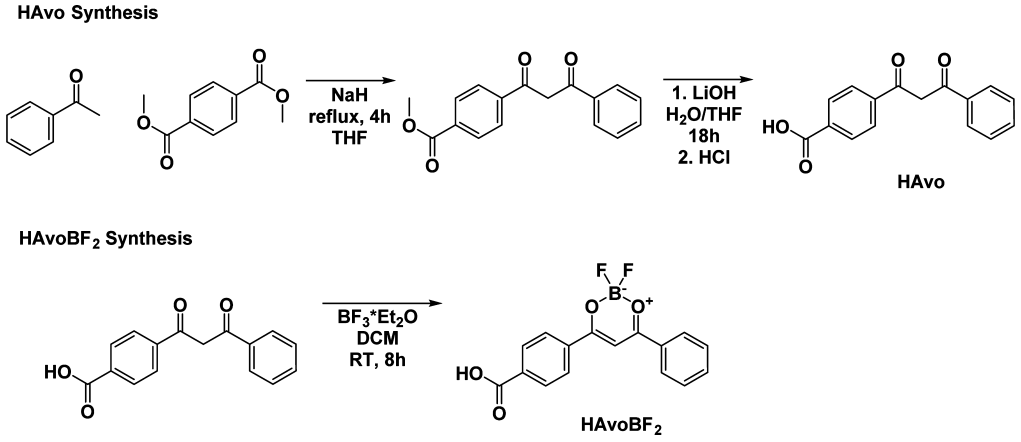

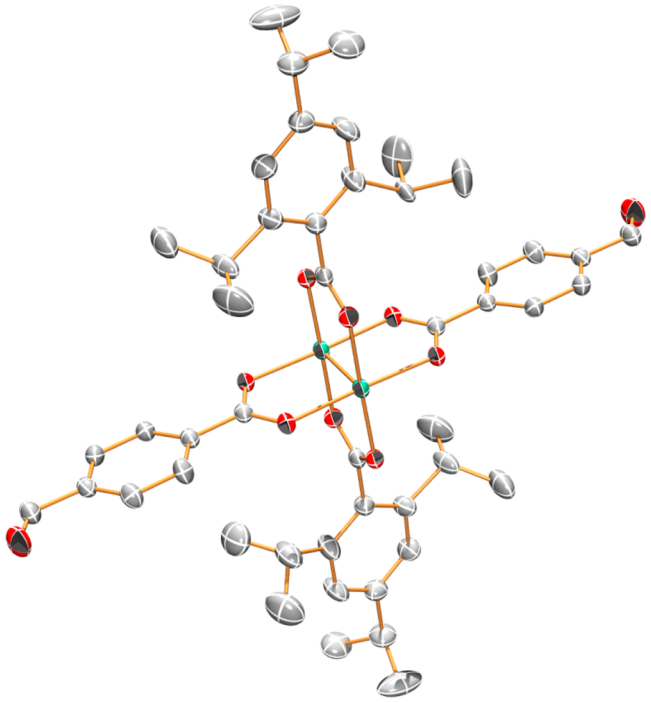

Figure 1. Molecular structure of **I** drawn at 50% probability, where blue = molybdenum, scarlet = oxygen, and gray = carbon. Hydrogens, solvent, and disorder are omitted for clarity.

Supporting Information Figure S5 (the enol form is shown later in Figure 2). In the keto form, the methylene unit separating the two ketonic groups removes the potential for extended conjugation and results in an electronic structure similar to **I**′.

Because of the forced planarity in both the enol form of **II**′and **III**′, it is appropriate to compare their respective calculations. The frontier molecular orbitals are compared in Figure 2. Here, the conjugation is extended further along the now planar trans ligands. In both molecules, the HOMO is principally the $Mo_2\delta$ orbital, and the LUMO and LUMO+1 are ligand π^* combinations. The presence of the BF_2 group in **III**′ significantly lowers the energy of these π^* orbitals, which reduces the HOMO−LUMO gap by ∼0.4 eV. The time-dependent DFT calculations predict that the lowest energy transition involves these orbitals and is ^{1}MLCT in nature. The $Mo_2\delta^*$ orbital is the LUMO+2 and is expected to be masked by the proximity of the intense ^{1}MLCT.

It is also worthy of note that the predicted HOMO−LUMO gaps of the keto and enol forms of **II**′ differ by only 0.15 eV and that the time-dependent DFT calculations predict their ^{1}MLCT transitions to differ by only 15 nm. However, the enol form of the ligand is predicted to have a ligand-based transition, a $\pi \rightarrow \pi^*$ transition at ∼350 nm, whereas the keto form has its $\pi \rightarrow \pi^*$ transition at higher energy, ∼290 nm. This makes a notable difference between the two forms of compound **II**. This has been observed experimentally with similar, but unchelated, avobenzone derivatives.[5] A comparison of frontier MOs for the enol and keto forms of **II**′ is shown in the Supporting Information, Figure S6.

Frequency analysis calculations pertaining to predicted infrared active bands are discussed later when time-resolved IR studies are presented.

^{1}H NMR Spectra. ^{1}H NMR spectra were recorded in THF-d_8, and the data are given in the Experimental part of the Supporting Information. The only point of emphasis or note at this juncture is that compound **II** appeared to exist in only the enol form, >97%, as evidenced by the hydroxyl proton resonance at ∼17.2 ppm and the CH proton at ∼7.3 ppm. The keto protons are expected to appear at 4.7−5.0 ppm; however, there is no signal in that region (Supporting Information Figure S4). In addition, the integration for the CH proton at ∼7.3 ppm agrees well with the integration of the other aromatic protons, which supports the equilibrium's being shifted almost entirely to the enol form.

The free ligand, HAvo, was also analyzed with ^{1}H NMR in THF-d_8, which showed that the molecules were present in ∼3% keto form, as evidenced by a peak at 4.75 ppm. When attached to the Mo_2 center in THF-d_8, this ground state equilibrium shifts overwhelmingly toward the enol.

UV−Visible Spectroscopy. The photostability of compound **II** and its ligand (HAvo) were investigated by photoexitation of 365 nm light over a period of 25 h while monitoring by UV−vis spectroscopy (Figure 3). Both solutions were standardized to have the same intensity of absorption at 350 nm. The spectra were taken in UV−vis cuvettes sealed with Kontes tops in degassed THF at room temperature. Over the course of the experiment, the absorption of HAvo decreases at 350 nm (typical of the enol form of these molecules). This decrease occurs concurrently with the formation of a new band at 245 nm. This new band is persistent and does not disappear after 24 h without UV irradiation (Supporting Information Figure S7). In other studies,[4] the growth of a band at 245 nm

DOI: 10.1021/jacs.5b01495
J. Am. Chem. Soc. 2015, 137, 5155−5162

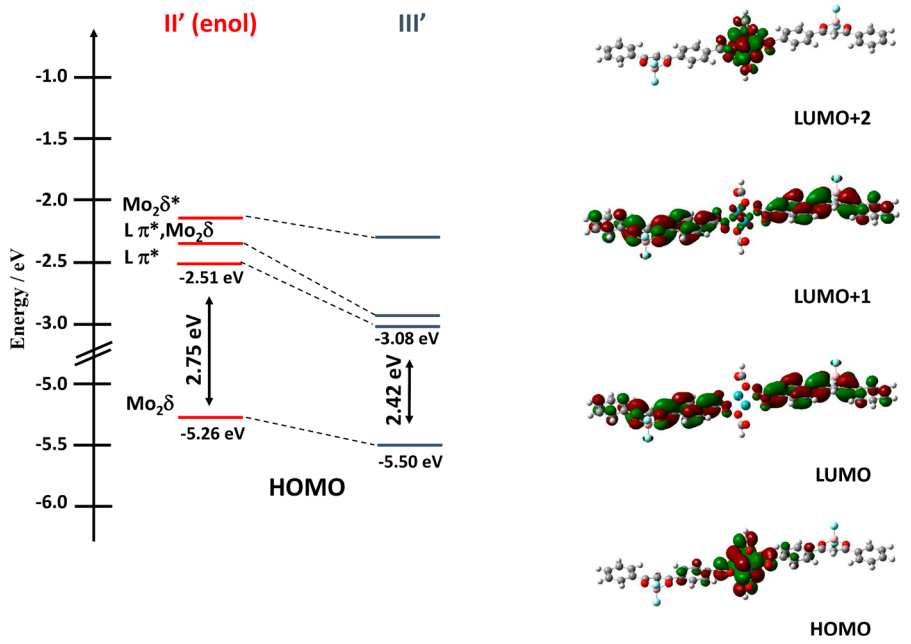

Figure 2. Frontier molecular orbital energy level diagram of the enol form of model compound **II**′ (left) and **III**′ (right), along with Gaussview 5.0.8 plots of **III**′ (isovalue = 0.2).

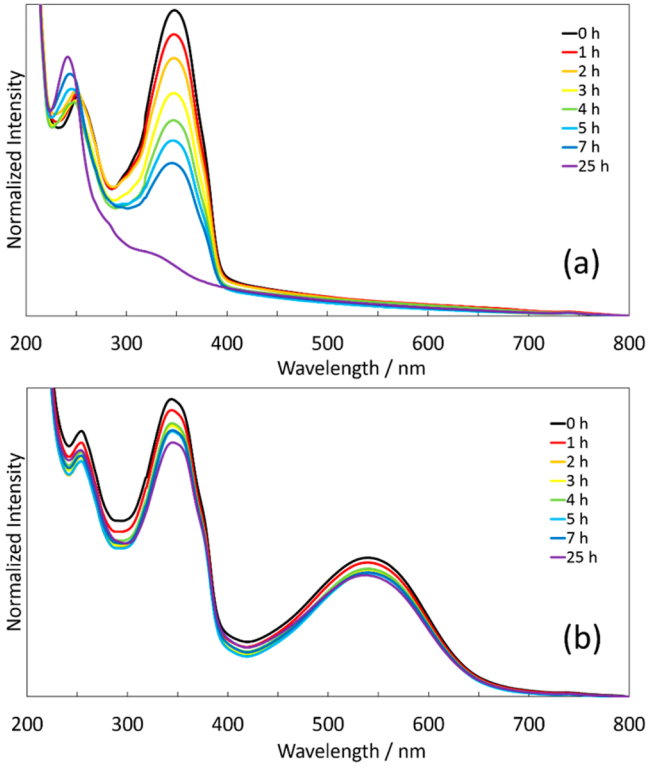

Figure 3. (a) UV/vis spectra of HAvo in THF under irradiation, λ_{ex} = 365 nm, taken at different time intervals. (b) UV/vis spectra of **II** in THF under irradiation, λ_{ex} = 365 nm, taken at different time intervals.

can be assigned to either the keto form of the ligand or the decomposition products of the ligand. However, when the keto form is left in the dark, it will thermally convert back to the enol form. Therefore, this band is indicative of photodecomposition.

This is in contrast to the absorbance of compound **II** under the same conditions. The decrease in absorption of compound **II** is much less than that of HAvo and occurs at a drastically reduced rate. There appears to be a slight blue shift of the ^{1}MLCT absorption after 25 h; however, this shift is slight and does not appear to recover in the dark. In addition, the absorbance of the Mo_2 complex underwent a uniform decrease both under illumination and in the dark (Supporting Information Figure S8). The cause of the decrease in absorption is assigned to the decomposition of the Mo_2 quadruple bond by a slow leak of oxygen into the cuvette over the course of 2 days.

A similar photolysis experiment was carried out under illumination with 254 nm light over the course of 4 h (Supporting Information Figures S9–S12). The absorbance of HAvo decreased more readily during this time and did not recover after 16.5 h in the dark. However, there was no formation of a band at 245 nm. This again shows that the decomposition products were formed, but with the increased energy of light, degeneration of the molecular structure of HAvo most likely occurred to a greater extent.

Even under these more stringent conditions, compound **II** was shown to be more robust than HAvo, with the absorbance decreasing only slightly over the course of 4 h. This decrease is also associated with a blue shift of the λ_{max} of the ^{1}MLCT from 540 to 517 nm. Over the course of 16.5 h in the dark, compound **II** underwent a slight decrease of absorption, which is again attributed to a slow leak of oxygen into the flask. During this time, the λ_{max} of the ^{1}MLCT absorption underwent a red shift by ∼5 nm. The blue shift in absorption caused by the irradiation of 254 nm light is assigned to the light-activated tautomerization of the Avo ligands on the Mo_2 center from the enol form to the keto. The subsequent red shift in the dark is assigned to the thermal recovery of the keto form back to the enol. The amount of tautomerization in compound **II** is small under prolonged illumination with 254 nm light and occurs even less (if at all) with 365 nm light. Notably, in both experiments, compound **II** underwent significantly less decomposition than HAvo. It should be emphasized that the purpose of sunscreen is to absorb at ∼350 nm, where

DOI: 10.1021/jacs.5b01495
J. Am. Chem. Soc. 2015, 137, 5155−5162

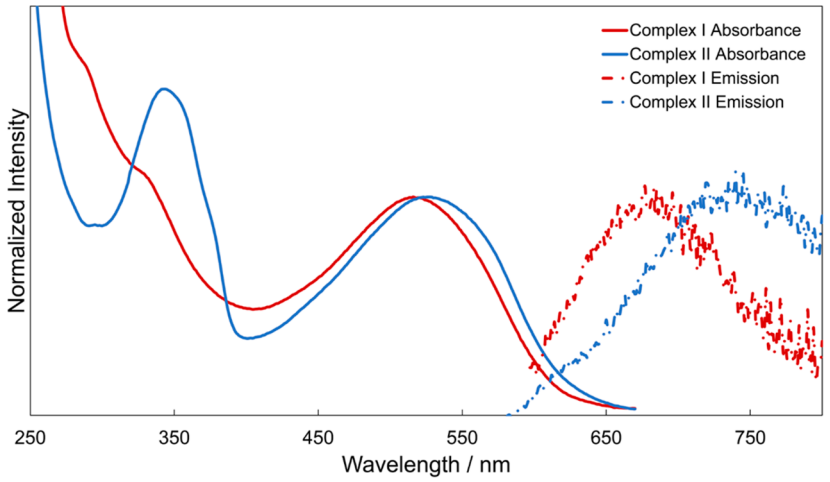

Figure 4. Electronic absorption and emission spectra (λ_{ex} = 520) of compounds **I** and **II** in THF at RT.

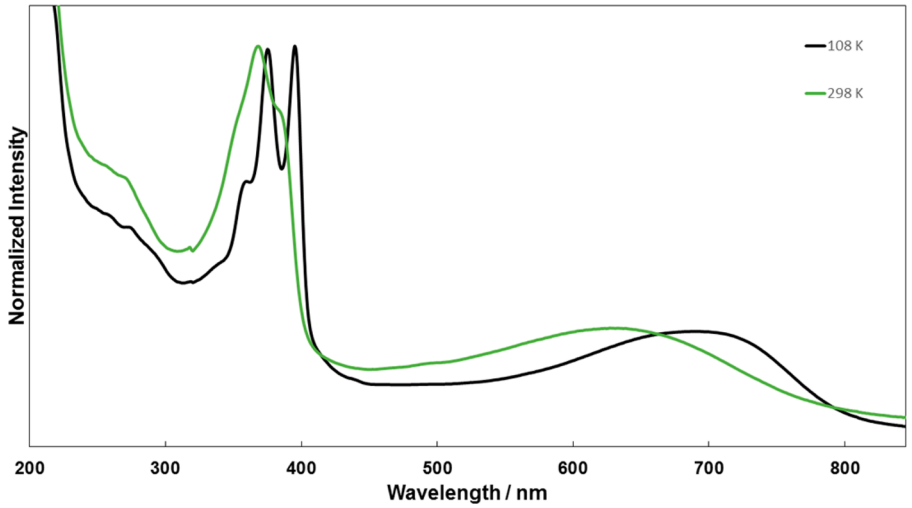

Figure 5. Electronic absorption spectrum of compound **III** in THF at 298 K (green) and 108 K (black).

compound **II** was shown to decompose only slightly over the course of irradiation after 25 h.

Figure 4 compares the UV−vis spectra of compounds **I** and **II** recorded in THF at room temperature, along with their steady state emission spectra. Both compounds show strong absorption at ∼520 nm, corresponding to their respective ^{1}MLCT transitions.

Of note is that compound **II** has a slightly lower energy absorption, as predicted, although the similarity is strong. However, the prominent absorption at 350 nm in **II** contrasts markedly with that for **I** and is characteristic of the enol form of the ligand. In addition, in comparing the spectra shown in Figure 4, we note that compound **II** displays a larger Stokes shift by ∼1100 cm^{-1} (4400 cm^{-1} vs 5500 cm^{-1} for compounds **I** and **II**, respectively). This implies that there is a greater structural rearrangement in the photoexcited state of compound **II** relative to **I**.

In THF, compound **III** shows a broad electronic transition centered around 650 nm. As shown in Figure 5, this is notably red-shifted compared with compound **II**. The ligand-based $\pi \rightarrow \pi^*$ transition is also more intense and shifted to longer wavelength. Compound **III** shows weak fluorescence at ∼850 nm which, regrettably, is in the range that falls between our visible and near-IR detectors. However, all these compounds show phosphorescence in the near-IR at ∼1060 nm (Supporting Information Figure S13). This is characteristic of emission from the ^{3}MoMo$\delta\delta^*$ state.[17]

Transient Absorption Spectroscopy. All three compounds have been examined by femtosecond and nanosecond transient absorption spectroscopy in THF solutions and a summary of the photophysical results can be seen in Table 1.

Table 1. Summary of the Lifetimes and State Assignments for Compounds I, II, and III

compd	S_1 lifetime (ps)	S_1 assignment	T_1 lifetime (μs)	T_1 assignment
I	5	^{1}MLCT	64	$^3\delta\delta^*$
II	13	^{1}MLCT	63	$^3\delta\delta^*$
III	15	^{1}MLCT	7	$^3\delta\delta^*$

The fsTA spectra, λ_{ex} = 568 nm, associated with **I** are shown in the Supporting Information. There is a significant transient at 380 nm that decays in ∼5 ps, which corresponds to the S_1 lifetime. The ground state bleach at 520 nm persists as the T_1, ^{3}MoMo$\delta\delta^*$ state is formed, which on the basis of the nanosecond spectra has a lifetime of 64 μs. The nsTA spectra for all three compounds along with the kinetic traces can be found in the Supporting Information.

DOI: 10.1021/jacs.5b01495
J. Am. Chem. Soc. 2015, 137, 5155−5162

Compound **II** was examined with irradiation into the MLCT and at higher energy into the ligand $\pi \rightarrow \pi^*$ transition. Qualitatively, the spectra are equivalent. The spectra obtained with 350 nm excitation are shown in the Supporting Information, and those with irradiation into the ^{1}MLCT are given in Figure 6 (top).

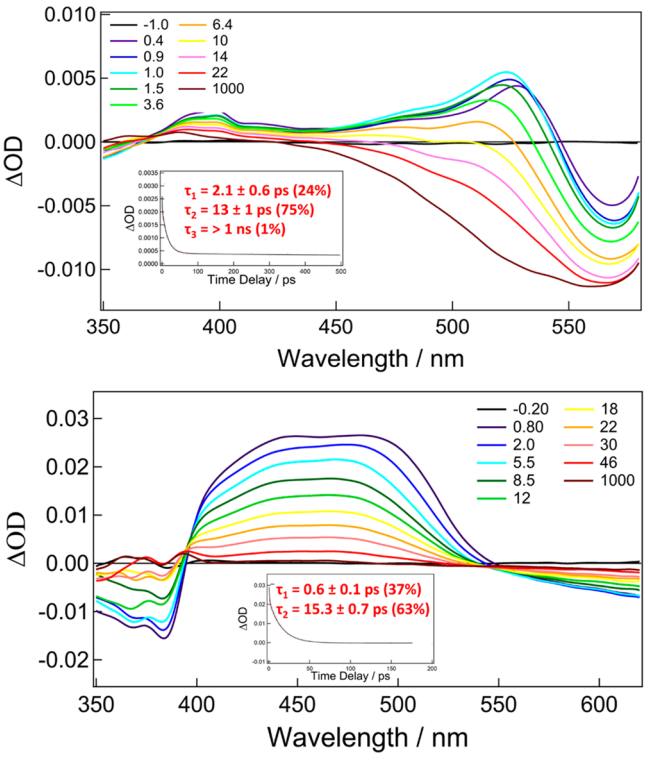

Figure 6. Top: fsTA spectra of **II** in THF at RT, λ_{ex} = 568 nm, with kinetic trace taken at 540 nm shown in the inset. Bottom: fsTA spectra of **III** in THF at RT, λ_{ex} = 650 nm, with kinetic trace taken at 500 nm shown in the inset.

At short times, we observe a transient at 520 nm, which appears to shift slightly to shorter wavelength as the ground state bleach decays. There is also a higher energy transient at ~380 nm, which decays with time but leaves a residual absorption at ~370 nm. Collectively, we can estimate the S_1 lifetime of the ^{1}MLCT state as 13 ps and the ^{3}MoMo$\delta\delta^*$ lifetime as 63 μs (from the femtosecond and nantosecond spectra, respectively).

The fsTA spectra for **III** are shown in Figure 6 (bottom) and are notable in that the transient at ~475 nm is 2 orders of magnitude more intense relative to those of **I** and **II**. The lifetime of the S_1 ^{1}MLCT state is 15 ps, and that of the T_1 ^{3}MoMo$\delta\delta^*$ state is 7 μs.

Time-Resolved Infrared Spectroscopy. Computational methods were used to aid in the assignment of the features associated with the fsTRIR data. In particular, frequency analysis calculations on the anions **I**′$^-$, **II**′$^-$(enol), **II**′$^-$(keto), and **III**′$^-$ were used for the assignment of the singlet features. This approximation works to simulate an additional electron residing on the carboxylate ligands after photoexcitation. The fsTRIR spectra for compound **I**, λ_{ex} = 568 nm, are shown in Figure 7 for the region 1750−1450 cm^{-1}. The ground state spectrum is depicted by the black dotted line.

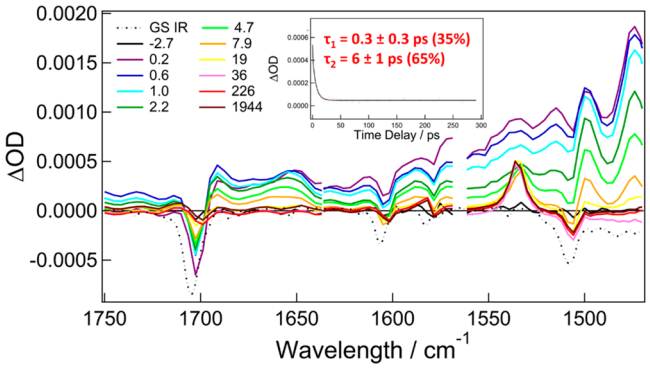

Figure 7. fsTRIR spectra of **I** in THF at RT, λ_{ex} = 568 nm, with kinetic trace taken at 1588 cm^{-1} shown in the inset.

Upon excitation, we observe the bleach of ν(C═O) at 1705 cm^{-1}, corresponding to the depletion of the ν(C═O), and the appearance of two transient bands at 1690 and 1655 cm^{-1} which may be assigned to $\nu(C{=}C)_{ring}$ stretches in the photoexcited state. The frequency analysis of **I**′$^-$ shows the highest energy stretch in the region, 1750−1450 cm^{-1}, is associated with ν(C═O). At lower energy, we also see the bleach of $\nu_{as}(CO_2)$ at 1505 cm^{-1} and the appearance of a band at ~1495 cm^{-1} assignable to $\nu_{as}(CO_2)$. These features are fairly typical of ^{1}MLCT states in metal carboxylates. The decay of these bands occurs within ~5 ps, consistent with fsTA measurements, to give rise to transient bands assignable to the ^{3}MoMo$\delta\delta^*$ state. Of particular note is the appearance of the 1540 cm^{-1} band, which is assignable to $\nu_{as}(CO_2)$ and arises from an electron being removed from the $Mo_2\delta$ orbital involved with backbonding to the ligand, causing the stretch to shift to higher energy. There is also a band at ~1580 cm^{-1}, most probably a C−C vibration of the ring, that represents some electron density still residing on the ligand at times >2 ns.

The fsTRIR spectra for compound **II**, λ_{ex} = 568, are shown in Figure 8 in the region 1750−1350 cm^{-1}. Again, the ground

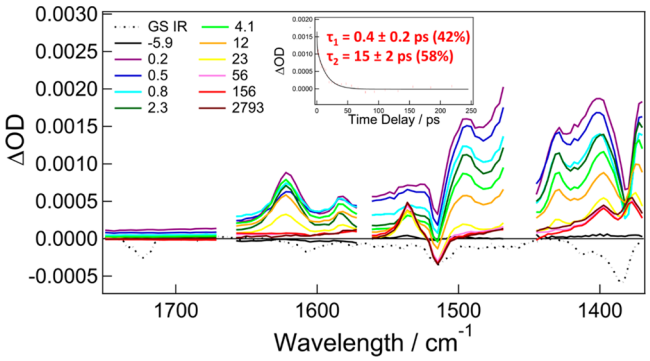

Figure 8. fsTRIR spectra of **II** in THF at RT, λ_{ex} = 568 nm, with kinetic trace taken at 1494 cm^{-1} shown in the inset.

state absorptions are depicted by the dotted black line. At high energy, the most notable feature in the transient IR spectrum is the absence of a band at ~1710 cm^{-1}. Ground state frequency analysis calculations indicate that the highest energy vibration in this region is one involving the hydrogen-bonded C═O moiety and the C−C of the ring for the enol form of **II**. Related calculations on the anions, **II**′$^-$(enol) and **II**′$^-$(keto), show that only the enol form lacks a stretching mode in this region, whereas the keto form exhibits a strong vibration at ~1700

DOI: 10.1021/jacs.5b01495
J. Am. Chem. Soc. 2015, 137, 5155−5162

cm^{-1} associated with ν (C═O). The early transient IR bands at ~1620 and 1580 cm^{-1} are most likely due to C−O and C−C coupled modes, and the band at 1490 cm^{-1} is assignable to $\nu_{as}(CO_2)$. Bleaches at 1385 and 1520 cm^{-1} are also observed and are due to the ground state depletion of $\nu_s(CO_2)$ and $\nu_{as}(CO_2)$, respectively. At longer time in the T_1 state, we again see the bleaches of these CO_2 stretches and the appearance of $\nu_{as}(CO_2)$ at ~1540 cm^{-1} indicative of the ^{3}MoMo$\delta\delta^*$ state.[17] In addition, the long-lived bands around 1400 cm^{-1} are likely due to $\nu_{as}(CO_2)$ stretches.

The fsTRIR spectra for compound **III** are shown in Figure 9. In comparison wtih **I** and **II**, the vibrational modes of **III** are

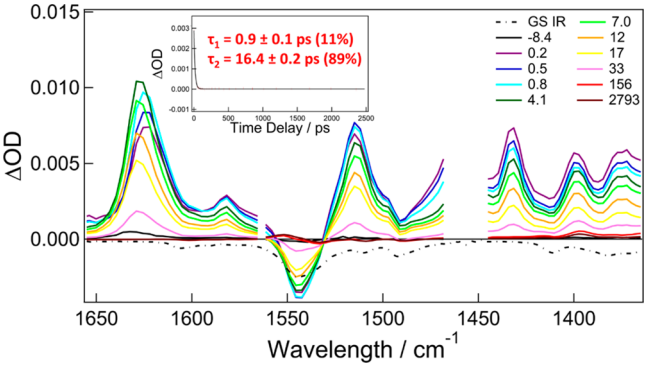

Figure 9. fsTRIR spectra of **III** in THF at RT, λ_{ex} = 650 nm, with the kinetic trace taken at 1582 cm^{-1} shown in the inset.

notably more intense in the ^{1}MLCT state. The absorptions at 1620 and 1580 cm^{-1} are similar to those seen for compound **II** and may similarly be assigned to C−O and C−C ring stretches. The strong bleach at 1544 cm^{-1} is associated with the C−O and C−C stretches in the ring containing the BF_2. This intense ground state absorption at 1544 cm^{-1} is not present in either **I** or **II**. The vibrations in the region of 1400 cm^{-1} are most probably symmetric C−C ring vibrations based on predictions of the calculated vibrational modes for **III**$'^-$. It appears that the introduction of the BF_2 unit enforces the planarity and greatly enhances the intensity of the ring vibrational modes at the expense of the carboxylate stretching vibrations. For example, in the T_1 state, the anticipated $\nu_{as}(CO_2)$ intensity at ~1540 cm^{-1} is significantly smaller relative to the ring vibration intensities.

CONCLUSIONS

As demonstrated in the fsTRIR data, compound **I** exhibits a transient feature assigned to ν (C═O), but compound **II** does not. This clearly shows that when λ_{ex} = 568 nm, **II** is in the enol form in the excited state; no presence of the keto is apparent. The ground state ^{1}H NMR similarly shows that the ground state equilibrium of compound **II** is >97% enol. The photolysis experiments indicate that there is significant enol-to-keto tautomerization at λ_{ex} = 254 nm after 4 h (see Supporting Information Figures S11 and S12), and there exists the potential for the same transformation at λ_{ex} = 365 nm, although to a much lesser extent. In all photolysis experiments, compound **II** proved to be more robust against UV light and did not decompose to the same extent as the free ligand HAvo.

Previous studies aimed at the deactivation of the photochemical conversion of avobenzone have involved substituent effects on the avobenzone ligand; however, these have not been able to eliminate the enol-to-keto tautomerization or the decomposition of the compound when exposed to UVA light. Herein, we have shown that the introduction of a heavy metal that has a lower energy ^{1}MLCT transition, with respect to the ^{1}LLCT, causes the higher energy transition to undergo rapid internal conversion to the ^{1}MLCT. The lower-energy ^{1}MLCT state then converts to the ^{3}MoMo$\delta\delta^*$ state within ~60 ps. This is in contrast to the avobenzone molecule that has been shown to form an excited state complex with a lifetime ~500 ns, which will lead to both tautomerization and decomposition (see Supporting Information Figures S9 and S10, which shows that the avobenzone derivative has decomposed by ~90%).[18] Although compound **II** is air-sensitive and, thus, could not be employed in sunscreens, we propose that attaching the avobenzone ligand to a metal that has a lower-energy ^{1}MLCT state could prevent the decomposition of avobenzone and its derivatives by providing a faster means of energy deactivation.

All compounds have singlet lifetimes, τ ~ 5−20 ps, which are quite long for S_1 states in ^{1}MLCT complexes, although not unusual for Mo_2 complexes. The triplet lifetimes, τ ~ 7−64 μs, is rather typical of ^{3}MoMo$\delta\delta^*$ states.[17] Compound **III** is unique in that it exhibits excited state absorptions with both fsTA and fsTRIR spectra ~100 times as intense as the usual spectra attributable to the enforced planarity of the ligand by the BF_2 moiety. Arylboron ligands, such as **III**, have been shown to provide interesting and unique photophysical properties. Similar compounds involving the same ligands with a W_2 metal core as well as some BODIPY derivatives are under further investigation.

ASSOCIATED CONTENT

Supporting Information

Materials and methods, synthesis, and characterization; crystallographic information, molecular orbital diagrams, photolysis spectra, near IR emission spectra, nanosecond and femtosecond transient absorption spectra. This material is available free of charge via the Internet at http://pubs.acs.org.

AUTHOR INFORMATION

Corresponding Authors

*E-mail: chisholm@chemistry.ohio-state.edu
*E-mail: gustafson.5@osu.edu

Notes

The authors declare no competing financial interest.

ACKNOWLEDGMENTS

We thank the National Science Foundation for funding on Grant Nos. CHE-1266298 and CHE-0957191 and the Ohio Supercomputer Center for computational resources. We are grateful to the Ohio State University Center for Chemical and Biophysical Dynamics for use of the laser systems, Professor Claudia Turro for use of instrumentation, and the CCIC Mass Spectrometry and Proteomics Lab for use of the MALDI, supported by NIH Award Nos. 1 S10 RR025660-01A1 and P30 CA016058.

REFERENCES

(1) Zawadiak, J.; Mrzyczek, M. *Spectrochim. Acta. A* **2012**, *96*, 815.
(2) Pinto da Silva, L.; Ferreira, P. J. O.; Duarte, D. J. R.; Miranda, M. S.; Esteves da Silva, J. C. G. *J. Phys. Chem. A* **2014**, *118*, 1511.
(3) Kikuchi, A.; Oguchi, N.; Yagi, M. *J. Phys. Chem. A* **2009**, *113*, 13492.

DOI: 10.1021/jacs.5b01495
J. Am. Chem. Soc. 2015, 137, 5155−5162

(4) Mturi, G. J.; Martincigh, B. S. *J. Photochem. Photobiol. Chem.* **2008**, *200*, 410.
(5) Paris, C.; Lhiaubet-Vallet, V.; Jiménez, O.; Trullas, C.; Miranda, M. Á. *Photochem. Photobiol.* **2009**, *85*, 178.
(6) Yamaji, M.; Kida, M. *J. Phys. Chem. A* **2013**, *117*, 1946.
(7) Afonso, S.; Horita, K.; Sousa e Silva, J. P.; Almeida, I. F.; Amaral, M. H.; Lobão, P. A.; Costa, P. C.; Miranda, M. S.; Esteves da Silva, J. C. G.; Sousa Lobo, J. M. *J. Photochem. Photobiol., B* **2014**, *140*, 36.
(8) Gaspar, L. R.; Tharmann, J.; Maia Campos, P. M. B. G.; Liebsch, M. *Toxicol. In Vitro* **2013**, *27*, 418.
(9) Butler, J. M.; George, M. W.; Schoonover, J. R.; Dattelbaum, D. M.; Meyer, T. *J. Coord. Chem. Rev.* **2007**, *251*, 492.
(10) Chisholm, M. H. *Coord. Chem. Rev.* **2015**, *282*−*283*, 60.
(11) Alberding, B. G.; Chisholm, M. H.; Gallucci, J. C.; Ghosh, Y.; Gustafson, T. L. *Proc. Natl. Acad. Sci. U.S.A.* **2011**, *108*, 8152.
(12) Brown-Xu, S. E.; Chisholm, M. H.; Durr, C. B.; Lewis, S. A.; Naseri, V.; Spilker, T. F. *Chem. Sci.* **2013**, *4*, 2105.
(13) Brown-Xu, S. E.; Chisholm, M. H.; Durr, C. B.; Spilker, T. F.; Young, P. J. *Dalton Trans.* **2013**, *42*, 14491.
(14) Loudet, A.; Burgess, K. *Chem. Rev.* **2007**, *107*, 4891.
(15) Sakai, A.; Tanaka, M.; Ohta, E.; Yoshimoto, Y.; Mizuno, K.; Ikeda, H. *Tetrahedron Lett.* **2012**, *53*, 4138.
(16) Nakatani, K.; Shirai, J.; Sando, S.; Saito, I. *J. Am. Chem. Soc.* **1997**, *119*, 7626.
(17) Chisholm, M. H.; Gustafson, T. L.; Turro, C. *Acc. Chem. Res.* **2012**, *46*, 529.
(18) Cantrell, A.; McGarvey, D. J. *J. Photochem. Photobiol., B* **2001**, *64*, 117.

DOI: 10.1021/jacs.5b01495
J. Am. Chem. Soc. 2015, 137, 5155−5162